Supporting Information

Catalytic CO oxidation over well-defined cobalt oxide nanoparticles: size-reactivity correlation

Viacheslav Iablokov[†], Roland Barbosa[†,‡], Glenn Pollefeyt[§], Isabel Van Driessche[§], Sergey Chenakin[†], and Norbert Kruse[†,‡]

[†] Chemical Physics of Materials, Université Libre de Bruxelles, Campus Plaine, CP 243, Brussels, B-1050, Belgium

[§] SCRiPTS, Dep. Inorganic and Physical Chemistry, Ghent University, Krijgslaan 281 - S3, 9000 Ghent, Belgium

[‡] Voiland School of Chemical Engineering and Bioengineering, Washington State University, Wegner Hall 155 A, Pullman, WA 99164-6515, USA

Corresponding Author: Norbert.Kruse@wsu.edu

I. Synthesis of model catalysts and catalytic tests.

The detailed procedure of monodisperse cobalt nanoparticles' (NPs) preparation has been described previously in Ref. [1] Briefly, the synthesis was carried out in a 3-neck 250 mL flask with an internal thermocouple through septa. Upon the injection of cobalt carbonyl precursor (0.52 g in 3 mL dichlorobenzene (DCB)) into a flask containing 15 mL DCB and 0.15 mL oleic acid, the precursor decomposed immediately yielding monodisperse particles. The size of cobalt NPs can be adjusted by the temperature; it decreases with increasing temperature of injection. After 15 min refluxing, the particle synthesis was stopped by addition of 15 mL DCB to decrease the temperature, followed by precipitation/centrifugation and washing cycles twice in 2-propanol and, finally, redispersion in chloroform. Colloids of cobalt NPs in chloroform were added to a meso-cellular foam (MCF-17) and sonicated for 2 h, and then centrifuged to separate the silica-loaded Co NPs from the supernatant. MCF-17 was synthesized according to Ref.[2] The samples were dried in an oven at 100 °C for 2 h. Finally, samples with of about 2 wt% of cobalt nanoparticles intercalated into the MCF-17 host were obtained (denoted as Co/MCF-17). Accurate weight loading was determined by atomic absorption spectroscopy (Perkin Elmer 3110, λ=240.7 nm). Prior to analysis, known amounts of Co/MCF-17 samples were dissolved in Aqua Regia under heating. Solutions were partially evaporated followed by addition of 0.12 M hydrochloric acid and quantitative transfer into analytical flasks. Then, AAS was conducted using a calibration line for cobalt metal. Cobalt loading was recalculated into cobalt oxide by taking into account a change in their molar masses (58.9 and 240.8 g mol^{-1}, respectively).

As prepared Co/MCF-17 samples were subsequently oxidized to obtain an active form of spinel-type cobalt oxide (hereafter denoted as Co_3O_4/MCF-17) using temperature-programmed oxidation (TPO) with 10% oxygen in argon at a total flow rate of 50 mL min^{-1} through an U-type reactor. Heating rates

of 6 °C min^{-1} were used up to 360 °C; oxidation was continued for 30 min at this temperature. The down-stream gas composition was continuously analysed by a quadrupole mass spectrometer (Balzers QME 200) using a calibrated flow-through-capillary. Gases were purchased from Praxair, Inc. with the following purities: O_2 (4.5), CO (4.7) and Ar (5.0).

A typical TPO profile is shown in Figure S1.

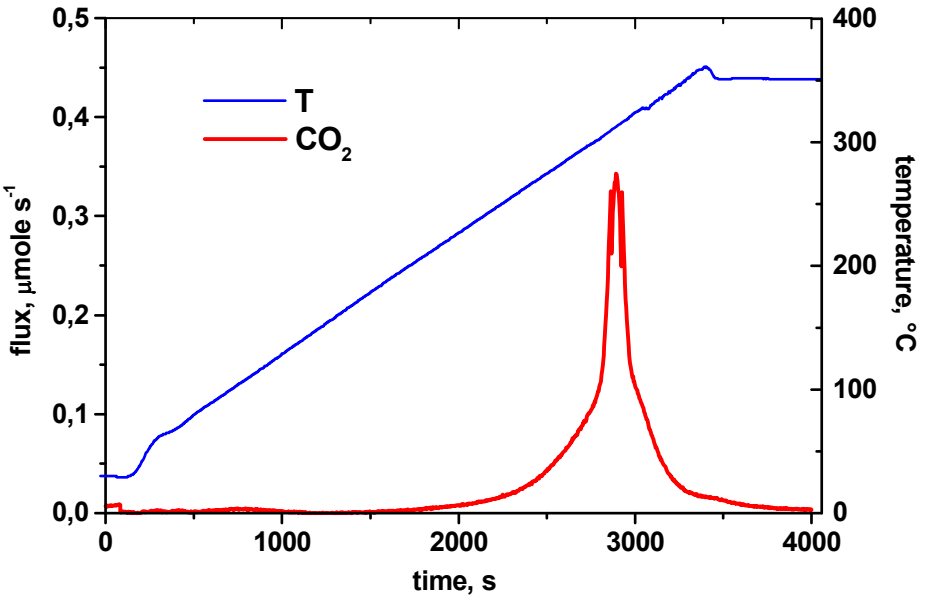

Fig. S1. TPO profile for Co/MCF-17 with Co particles size of 4.5 nm

The thermally activated decomposition of oleic acid remainders at the surface of cobalt NPs starts at ~ 230 °C and leads to a maximum release of CO_2 gas at around 300 °C for all sizes. Water is likewise produced during TPO; the slow elution through the fixed bed and in the capillary of the mass spectrometer causes the m/e=18 signal to extend nearly over the entire temperature range with now clear peak appearing.

(HR)TEM imaging of Co NPs was performed using a Jeol 2100 microscope with a LaB_6 source as well as a Cs-corrected Jeol JEM 2200 FS microscope operating both at an accelerating voltage of 200 kV. Samples were diluted in chloroform, and then dripped onto the Cu grids.

For closer inspection of the possible morphology change due to faceting in the case of large particles, a colloid containing 9.6 nm cobalt particles was deposited on a silicon wafer (111) using Langmuir-Blodgett technique (Nima Technology, M611).[3] A drib of the colloid in chloroform was dropped onto the water surface of the tray. An increase in the surface tension allowed formation of a monolayer of the nanoparticles. The layer was deposited onto a silicon wafer using its horizontal liftoff move (initially,

the wafer was located in the underwater position). The obtained monolayer of cobalt particles was oxidized following the TPO procedure. As is highlighted by SEM analysis (Figure S2), cobalt oxide particles 11.6 nm in size appeared in a polyhedral shape.

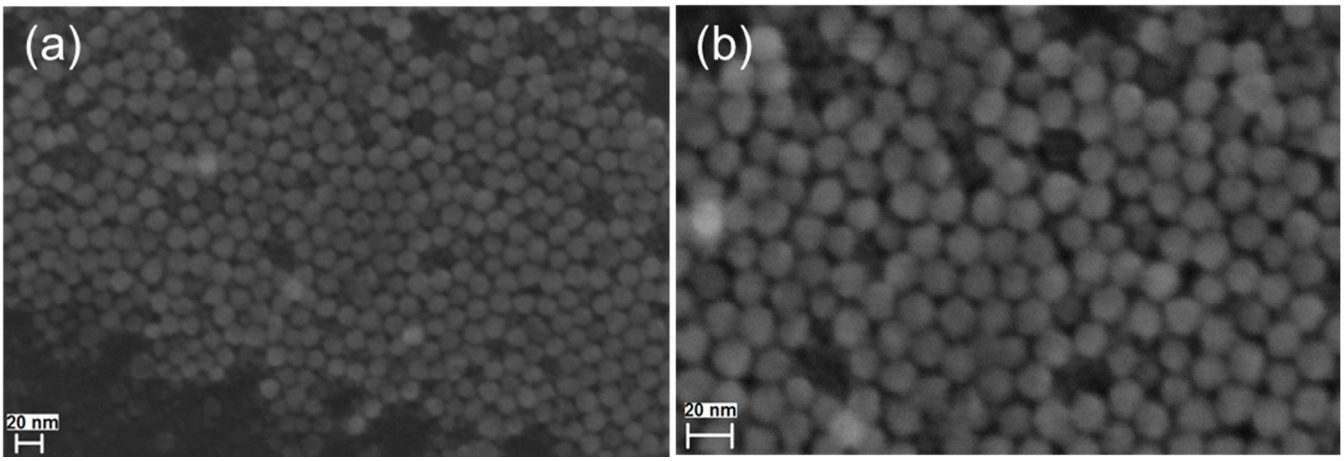

Fig. S2. (a) SEM image of a monolayer of 11.6 nm cobalt oxide particles on silicon wafer; (b) higher magnification.

Catalytic tests were performed after TPO. The same U-type reactor was used for these tests, i.e. samples had not to be displaced to another dedicated device. Accordingly, the gas flow was switched to a mixture of CO and O_2 (2% each) using Ar as vector gas. The total flow rate was adjusted to 50 mL min^{-1} at overall atmospheric pressure. The temperature was raised (5 °C min^{-1}) in increments with time intervals of 20 min between successive incremental increases. The CO oxidation reaction was carried out under steady-state conditions at 150 °C. CO conversion was calculated from the measured amount of formed CO_2.

II. Calculation of reaction rate

The surface area of the particles (m^2 g^{-1}) is calculated as $S = \frac{6}{\rho \times R}$, where ρ is the density of cobalt oxide ($6.11 \cdot 10^6$ g m^{-3}), and R is the particle size (m) assuming spherical geometry. Consequently, the surface reaction rate (nm^{-2} s^{-1}) can be calculated by dividing the reaction rate in terms of mole g^{-1} s^{-1} by the total specific surface area, S, i.e. $r_{surface} = \frac{N_A \times r}{S \times 10^{18}}$. We do not calculate turnover frequencies here since the exact nature of the catalytically active site is not known (despite Co^{3+} playing a dominate role, as shown in this paper).

Table S1. Reaction rates versus size of cobalt oxide nanoparticles.

Co size, nm	Co_3O_4 size, nm	Reaction rate, μmole g^{-1} s^{-1}	Reaction rate, nm^{-2} s^{-1}
3.2	3.5	154.3	0.33
3.7	4.2	191.1	0.49
4.5	5.2	246.2	0.78
5.8	6.8	175.0	0.73
6.8	8.0	142.4	0.70
8.1	9.6	69.1	0.41
9.6	11.6	21.6	0.15
10.2	12.3	13.8	0.10

III. XPS studies

X-ray photoelectron spectroscopy (XPS) experiments were performed at a base pressure of $<5\times10^{-10}$ mbar, using Mg Kα radiation at an operating source power of 13 kV×11 mA. XP spectra were acquired with a hemispherical energy analyzer in a constant pass energy mode at E_p = 50 eV with an energy step of 0.075 eV. After subtraction of the Shirley-type background, the core-level spectra were decomposed into components with mixed Gaussian-Lorentzian lines using a non-linear least-squares curve-fitting procedure (CASA XPS software). XPS measurements were carried out for Co NPs of varying size deposited onto a gold foil and annealed in a flow of 10% O_2 with argon as balance using the same temperature-programmed oxidation procedure as for the preparation of Co_3O_4/MCF-17 catalysts.

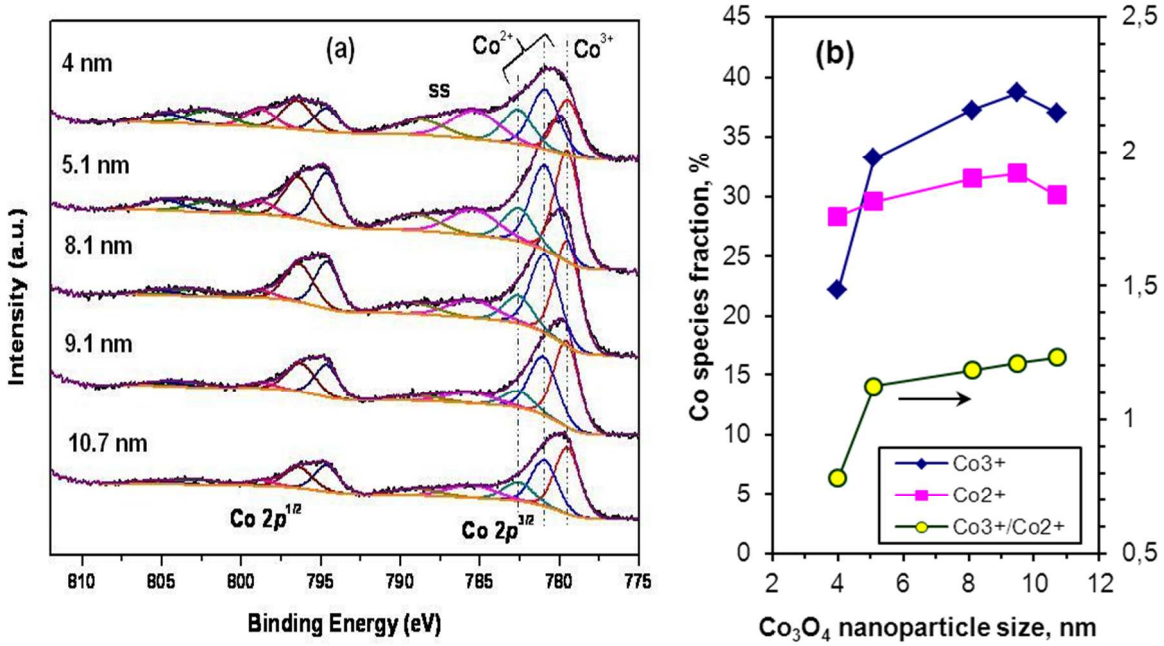

Fig. S3. (a) XP core-level Co 2p spectra of cobalt oxide nanoparticles of various sizes; (b) variation of Co species fractions and their ratio as a function of Co NP size.

Figure S3 (a) shows the Co 2p spectra for cobalt oxide nanoparticles of varying size which exhibit a doublet with a spin-orbit splitting of about 15.2 eV. The deconvolution of the spectra revealed the occurrence of Co^{3+} and Co^{2+} states located at binding energies of 779.5±0.1 and 780.9±0.2 eV, respectively (for the Co $2p_{3/2}$ peak).[4] In view of the presence of Co^{2+} ions, an additional component related to multiplet splitting was used in the deconvolution. The occurrence of Co^{3+} and Co^{2+} ions along with characteristic shake-up satellites (SS) indicates formation of Co_3O_4 during oxidation of Co nanoparticles. The fractions of the components attributed to Co^{3+} and Co^{2+} species in the Co 2p envelope increase non-monotonously with increasing Co NP size and reach a maximum in the range around 9.5 nm (Figure S3 (b)). The Co^{3+}-to-Co^{2+} fraction ratio displays a steep rise in the range of 4-5 nm followed by a slight gradual increase in the range of sizes from 5 to 11 nm.

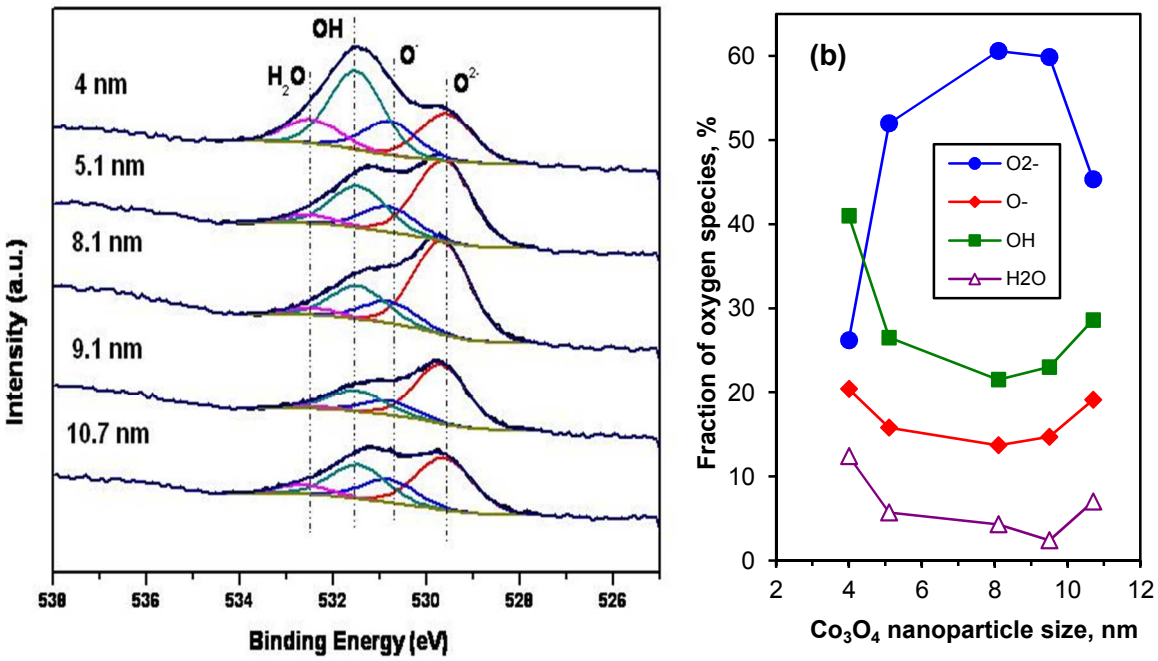

Fig. S4. (a) XP O 1s spectra of cobalt oxide nanoparticles of various sizes; (b) variation of O 1s species fractions as a function of Co NP size.

The shape of the O 1s spectra of cobalt oxide NPs turned out to be strongly dependent on the particle size (Figure S4 (a)). The O 1s spectra were fitted by using three and four components with equal FWHM. In the first case, the components located at 529.65 ± 0.02 eV, 531.18 ± 0.09 eV and 532.2 ± 0.17 eV were attributed to lattice ions O^{2-}, hydroxyl groups OH and adsorbed water, respectively. In the second approach (Figure S4 (a)), the components with binding energies of 529.62 ± 0.04 eV, 530.8 ± 0.05 eV, 531.48 ± 0.03 eV and 532.5 ± 0.06 eV were assigned to O^{2-} lattice ions, low-coordinated or adsorbed O^{-} ions, hydroxyl groups and adsorbed water, respectively. In both approaches, the fractions of these components in the O 1s envelope exhibit strong and similar variations as a function of NP size, demonstrating opposite trends for O^{2-} and OH species. As can be seen in Figure S4 (b), the fraction of the O^{2-} lattice ions increases non-monotonously and the fractions of the O^{-} ions, OH groups and adsorbed H_2O decrease non-monotonously with increasing NP size, attaining extreme values in the range of 8-9 nm.

C 1s spectra were also recorded and indicated the presence of various carbon-containing species. The deconvoluted spectra, not shown here, pointed to species with C–C, C–O and O–C=O bonds which most probably resulted from the interaction of the cobalt oxide particles with contaminations (e.g. hydrocarbons) in ambient air.

The valence bands of cobalt oxide NPs (Figure S5) were obtained by subtracting the spectrum of pure Au foil from the valence band spectra of the nanoparticles supported on gold. These spectra can be

compared with the valence band spectra of CoO and Co_3O_4 studied in references[4-7] The valence band of CoO was suggested[5] to consist of two Co 3d features at 1.8 eV (e_g α) and 3.8 eV (t_{2g} β) and a O 2p feature centered at 6.8 eV. According to Ref.[6], photoemission from the top of the valence band of CoO results from the $3d^7\underline{L}$ final state yielding a peak at 1.7 eV; an additional feature related to Co 3d orbitals with e_g character is observed at 3.8 eV. In Co_3O_4, a new, sharp valence-band peak at 1.0 eV (Co^{3+}octahedral) was found to develop which increased in intensity with oxidation at the expense of the 1.7 eV peak of the CoO substrate (Co^{2+} tetrahedral). Oxygen 2p-derived bands were observed at 5.1 and 7.6 eV. Also, oxygen species adsorbed at defect sites were suggested[7] to yield an O 2p band at around 4 eV.

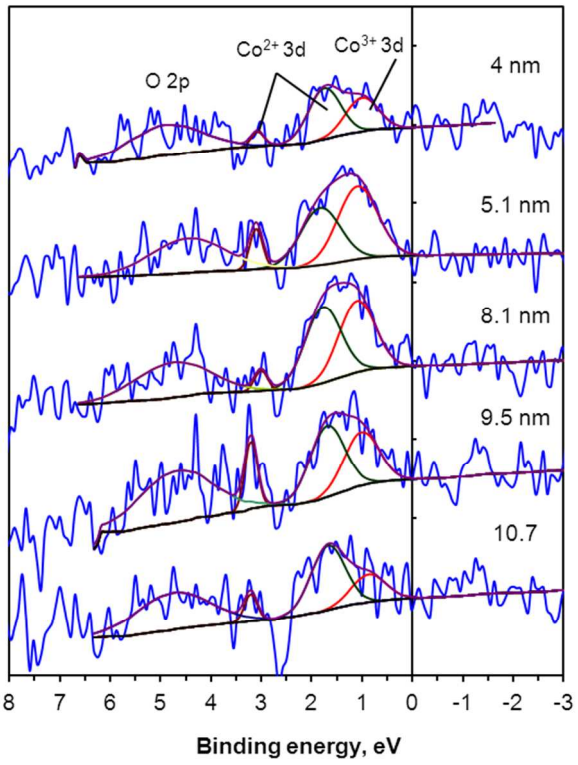

Fig. S5. Valence band spectra of oxidized cobalt nanoparticles of various size.

On the basis of these studies, we fitted the valence band spectra of oxidized cobalt NPs in a short energy range up to 6 eV by using four components (Figure S5) and obtained the peak positions (0.9-1.1 eV; 1.7-1.8 eV; 3.1-3.2 eV and 4.5-4.9 eV) which are in good agreement with the Co^{3+} 3d, two Co^{2+} 3d and O 2p (ads) band assignments.[5-7] The derived fractions (or spectral weights) of the Co^{3+} and O 2p states vary non-monotonuously and in an opposite way with Co NP size, displaying respectively a maximum and a minimum for cobalt oxide particles 5.1 nm in size. Note that the width of the Co^{3+} 3d band also peaks at 5.1 nm.

References

(1) Iablokov, V.; Beaumont, S. K.; Alayoglu, S.; Pushkarev, V. V.; Specht, C.; Gao, J.; Alivisatos, A. P.; Kruse, N.; Somorjai, G. A. *Nano Lett.* **2012**, *12*, 3091-3096.

(2) Han, Y.; Lee, S. S.; Ying, J. Y. *Chem. Mater.* **2007**, *19*, 2292-2298.

(3) Yang, P. *Nature* **2003**, *425*, 243-244.

(4) Chuang, T. J.; Brundle, C. R.; Rice, D. W. *Surf. Sci.* **1976**, *59*, 413-429.

(5) Kim, K. S. *Phys. Rev. B* **1975**, *11*, 2177-2185.

(6) Langell, M. A.; Anderson, M. D.; Carson, G. A.; Peng, L.; Smith, S. *Phys. Rev. B : Conden. Matter Mater. Phys.* **1999**, *59*, 4791-4798.

(7) Soriano, L.; Abbate, M.; Fernandez, A.; Gonzalez-Elipe, A. R.; Sirotti, F.; Sanz, J. M. *J. Phys. Chem. B* **1999**, *103*, 6676-6679.